

# Metallic Quantized Anomalous Hall Effect without Chiral Edge States

Kai-Zhi Bai,<sup>1</sup> Bo Fu,<sup>2</sup> Zhenyu Zhang,<sup>3</sup> and Shun-Qing Shen<sup>1,\*</sup>

<sup>1</sup>*Department of Physics, The University of Hong Kong, Pokfulam Road, Hong Kong, China*

<sup>2</sup>*School of Sciences, Great Bay University, Dongguan, China*

<sup>3</sup>*Hefei National Laboratory of Physical Sciences at the Microscale,  
University of Science and Technology of China, Hefei, Anhui 230026, China*

(Dated: August 14, 2023)

The quantum anomalous Hall effect (QAHE) is a topological state of matter with a quantized Hall resistance. It has been observed in some two-dimensional insulating materials such as magnetic topological insulator films and twisted bilayer graphene. These materials are insulating in the bulk, but possess chiral edge states carrying the edge current around the systems. Here we discover a metallic QAHE in a topological insulator film with magnetic sandwich heterostructure, in which the Hall conductance is quantized to  $e^2/h$ , but the longitudinal conductance remains finite. This effect is attributed to the existence of a pair of massless Dirac cones of surface fermions, with each contributing half of the Hall conductance due to quantum anomaly. It is not characterized by a Chern number and not associated to any chiral edge states. Our study offers novel insights into topological transport phenomena and topological metallic states of matter.

*Introduction-* QAHE is a quantum transport phenomenon in two-dimensional ferromagnetic materials where the Hall resistance is quantized to the von Klitzing constant  $h/e^2$  while the longitudinal resistance disappears [1–7]. The materials are band insulators in the bulk, and possess chiral edge states carrying a dissipationless electric current around the system boundary [8, 9]. The electronic band structures of the materials are characterized by the Chern number [10, 11], which equals the number of chiral edge states [12]. Over the last decade the effect has been observed experimentally in a series of topological insulator (TI) films and two-dimensional materials [13–24]. The picture of the chiral edge states are also confirmed experimentally [25, 26]. Recently the half-quantized Hall conductance was reported in a magnetic doped TI film [27]. The power-law decay of the Hall current indicates possible existence of distinct QAHE, which is not characterized by the Chern number or chiral edge state [28–30]. This provides a possible route to explore novel types of QAHE.

A TI film hosts a pair of massless Dirac cones of electrons near the two surfaces. The exchange interaction of magnetic ions or the ferromagnetic magnetization breaks time-reversal symmetry and may manipulate the nature of the surface states [31]. Here we propose a unique type of QAHE with no chiral edge states in a magnetically doped TI film in which the Hall conductance is quantized to be  $e^2/h$  while the longitudinal conductance is finite. The Hall resistivity is then not quantized. The magnetically doped layers are confined near the center to form a sandwich structure as illustrated in Fig 1. Based on numerical calculation and analytical analysis of the film, it is observed that increasing the concentration  $x$  of doped Cr atoms or increasing the Zeeman field may induce a transition of the Hall conductance from 0 to  $-e^2/h$  meanwhile the band structure shows that no energy gap opens as the magnetically doped layer is far

away from the top and bottom surfaces. Further analysis shows that the TI film hosts a pair of massless Dirac fermions, one carries  $e^2/2h$ , and another carries  $-e^2/2h$  of the Hall conductance in the absence of the Zeeman field. An increasing Zeeman field drives one of the gapless Dirac cones and an accompanying gapped Dirac cone to exchange their masses, and the sign of Hall conductance changes from  $e^2/2h$  to  $-e^2/2h$ . Consequently, the total Hall conductance becomes  $-e^2/h$  (the sign is determined by the direction of the Zeeman field). The longitudinal conductance is finite as no gap opens in the surface states, and has a minimal value when the chemical potential sweeps the Dirac point of the surface electrons. Hence there do not exist chiral edge states localized near the system boundary.

*Magnetic sandwich TI film-* We consider a symmetric TI film with a magnetic doped layer at the center  $m\text{QLX}_2\text{Te}_3/3\text{QLX}_{2-x}\text{Cr}_x\text{Te}_3/m\text{QLX}_2\text{Te}_3$  with  $X = (\text{Bi}, \text{Sb})$  and  $m = 4$  as shown in Fig. 1. A larger integer  $m$  does not change the main result in this proposal.  $\text{Bi}_2\text{Te}_3$  and  $\text{Sb}_2\text{Te}_3$  are prototypes of strong TIs [32]. 1QL means a quintuple layer of X and Te atoms, and is about  $1nm$  in  $\text{Bi}_2\text{Te}_3$ . The Dirac cone of surface states was observed explicitly by the ARPES [33, 34] and was also evidenced by a series of transport measurements. The exchange interaction between the p-orbital electron from Bi and Te and magnetic ions Cr may induce a finite magnetization in  $\text{X}_{2-x}\text{Cr}_x\text{Te}_3$  [2, 31]. Tuning the concentration  $x$  of Cr can change the exchange interaction, and even makes it a ferromagnetic insulator [35]. The magnetic element Cr was modulation-doped only near the center layer. The non-doped layers are thick enough such that the top and bottom surface electrons do not open energy gap. The topological nature of the band structures of  $\text{Bi}_2\text{Se}_3$  and  $\text{Bi}_2\text{Te}_3$  can be well described by the tight-binding model for the electrons of  $P_{z,\uparrow}$  and  $P_{z,\downarrow}$  orbitals from (Bi and Te or Se atoms near the Fermi energy [32, 36],

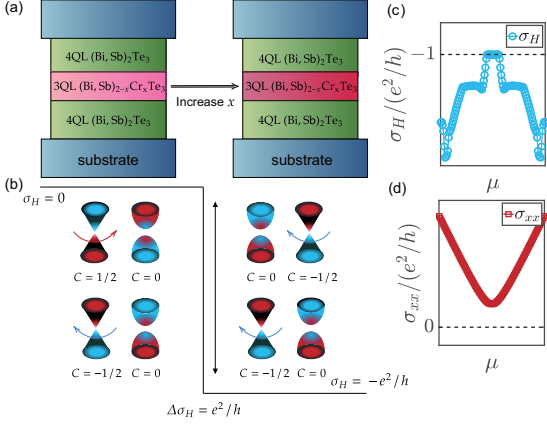


Figure 1. (a) Schematic of the magnetic sandwich heterostructure of a  $(\text{Bi, Sb})_2\text{Te}_3$  TI film with the concentration  $x$  of magnetically doped Cr atoms. (b) A transition from two pairs of massless and massive Dirac fermions with no net Hall conductance  $\sigma_H = 0$  at low concentration  $x$  to that with a quantized Hall conductance  $\sigma_H = -\frac{e^2}{h}$  at higher concentration  $x$  (the sign depending on the direction of magnetization).  $C$  represents the Hall conductance in the unit of  $e^2/h$ , while color represents the sign-value of the Berry curvature with blue for minus and red for positive. The masses of a pair of massless and massive Dirac fermions (at the upper horizontal row) at lower energy exchange by increasing the concentration  $x$  while the higher energy parts of the Dirac fermions remain almost unchanged. (c) Schematic of the quantized Hall conductance  $\sigma_{xy}$  and (d) the longitudinal conductivity  $\sigma_{xx}$  as function of the chemical potential  $\mu$  at a higher doping concentration  $x$ .

$$H_{TI} = \sum_l \Psi_l^\dagger \mathcal{M} \Psi_l + \sum_{l, \alpha=x, y, z} \left( \Psi_l^\dagger \mathcal{T}_\alpha \Psi_{l+\alpha} + \Psi_{l+\alpha}^\dagger \mathcal{T}_\alpha^\dagger \Psi_l \right) \quad (1)$$

where  $\mathcal{M} = (m_0 - 2 \sum_\alpha t_\alpha) \sigma_0 \tau_z$ ,  $\mathcal{T}_\alpha = t_\alpha \sigma_0 \tau_z - i \frac{\lambda_\alpha}{2} \sigma_\alpha \tau_x$ ,  $\Psi_l^\dagger$  and  $\Psi_l$  are the four-component creation and annihilation operators at position  $l = (l_x, l_y, l_z)$ . The Pauli matrices  $\sigma_\alpha$  and  $\tau_\alpha$  act on the spin and orbital indices, respectively. Adapting a model homogeneous in  $x - y$  plane leads to  $t_\parallel = t_x = t_y$ ,  $t_\perp = t_z$ ,  $\lambda_\parallel = \lambda_x = \lambda_y$ ,  $\lambda_\perp = \lambda_z$ . The magnetic effect induced by Cr is modeled by introducing the Zeeman field along the  $z$  direction,  $V_Z = \sum_l V_z(l_z) \Psi_l^\dagger \sigma_z \tau_0 \Psi_l$ .  $V_z(l_z) = \alpha t_\perp$  in the magnetic doped layers (using  $t_\perp$  as a unit) with  $l_z = \pm 1/2, \dots, \pm(m_z - 1)/2$  where film thickness  $L_z$  and the magnetic layer thickness  $m_z$  are assumed to be even ,

and equals zero in the non-doped layers. Here we ignore the possible change of the bulk gap  $m_0$  in  $X_{2-x}\text{Cr}_x\text{Te}_3$  caused by doping.

We consider the periodic boundary condition in the  $x$  and  $y$  direction. The band structure of the film is calculated numerically by means of the exact diagonalization method as shown in Fig. 2(a) in the absence of magnetic layers ( $\alpha = 0$ ) and (b) in the presence of magnetic layers ( $\alpha = 0.9$ ). It is observed that there exists a pair of massless Dirac fermions in both cases. The dispersions are doubly degenerated near the crossing point at  $k = 0$ . The presence of the Zeeman field  $\alpha$  does not open energy gap in the surface states while  $\alpha$  varies from 0 to 0.9. It is reasonable that the massless surface electrons are mainly located near the top and bottom surfaces which are far away from the magnetic ions in the magnetic layers (see Fig. S4 in Ref. [37]). After having the numerical energy eigenvalues and eigenvectors, the Hall conductance can be calculated numerically by means of the Kubo formula for electric conductivity [38]. The Hall conductance becomes nonzero in the presence of  $\alpha$  when the Fermi level crosses the conduction and valence bands with  $n > 1$ . As shown in Fig. 2(c), a plateau of zero Hall conductance appears near  $\mu = 0$  for a weak field, while for a strong Zeeman field  $\alpha$ , a flat plateau of  $\sigma_H = -\frac{e^2}{h}$  appears. Detailed calculation presented in Fig. 2(d) shows the Hall conductance changes from zero to  $-\frac{e^2}{h}$  with increasing the Zeeman field  $\alpha$  for fixed chemical potentials. Considering that there is no band gap while  $\alpha$  changes from 0 to 0.9, the longitudinal conductivity must be finite. Thus the appearance of the Hall conductance indicates that it differs from the conventional QAHE in an insulating phase.

*Equivalent Dirac-like fermions-* To explore the physical origin of the quantized Hall conductance, we study the band structure of the film in the presence of the Zeeman field. First we adopt the Fourier transformation  $\Psi_{l_z, \mathbf{k}} = \sum_{l_x, l_y} \exp[i l_x k_x + i l_y k_y] \Psi_{l_x, l_y, l_z}$ . The tight binding model in 1 with the Zeeman field  $H_{tot} = H_{TI} + V_Z$  can be split into two parts  $H_{tot} = H_\parallel + H_{1D}(\alpha)$ . The in-plane spin-orbital coupling  $H_\parallel = \sum_{l_z, \mathbf{k}} \Psi_{l_z, \mathbf{k}}^\dagger \lambda_\parallel (\sin k_x \sigma_x + \sin k_y \sigma_y) \tau_x \Psi_{l_z, \mathbf{k}}$ . The part  $H_{1D}(\alpha)$  for each  $\mathbf{k}$  is equivalent to a one-dimensional TI with the  $\mathbf{k}$ -dependent band gap  $m(\mathbf{k}) = m_0 - 4t_\parallel \left( \sin^2 \frac{k_x}{2} + \sin^2 \frac{k_y}{2} \right)$  in a Zeeman field. In the case,  $[\sigma_z, H_{1D}] = 0$  such that  $H_{1D}$  can be diagonalized to have a series of energy eigenvalues  $\tilde{m}_{n, \chi}(k_x, k_y)$  and eigenvectors  $\tilde{\Phi}_{\mathbf{k}, n, \chi} = \sum_{l_z} U_{n, \chi; l_z} \Psi_{l_z, \mathbf{k}}$  with  $n = 1, \dots, L_z$  and  $\chi = \pm$ . The double degeneracy is caused by time-reversal symmetry and inversion symmetry. Using the eigenvectors as a new basis, we find that  $H_{tot}$  is equivalently reduced to a series of two-dimensional Dirac-like models  $H_{tot} \equiv \sum_{\mathbf{k}, n, \chi = \pm 1} \tilde{\Phi}_{\mathbf{k}, n, \chi}^\dagger h_{n, \chi}(\mathbf{k}) \tilde{\Phi}_{\mathbf{k}, n, \chi}$  with

$$h_{n, \chi}(\mathbf{k}) = \lambda_\parallel (\sin k_x \sigma_x + \sin k_y \sigma_y) + \tilde{m}_{n, \chi}(\mathbf{k}, \alpha) \sigma_z. \quad (2)$$

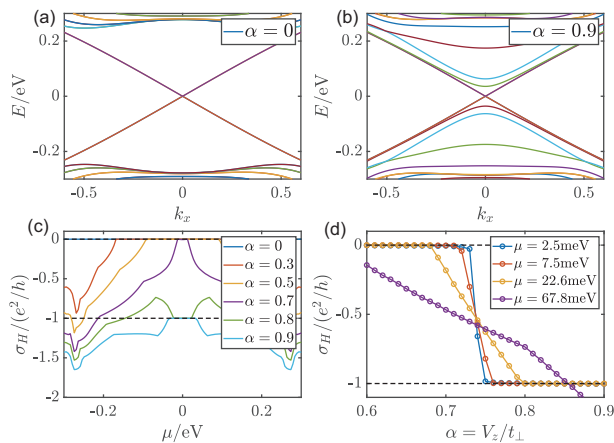


Figure 2. The band structure near the  $\Gamma$  point with  $k_y = 0$  (a) in the absence of magnetic doping ( $\alpha = 0$ ) and (b) in the presence of magnetic doping ( $\alpha = 0.9$ ). The gapless dispersions for the surface states in (a) and (b) are doubly degenerated. (c) The calculated Hall conductance as a function of the chemical potential  $\mu$ . (d) The Hall conductance as a function of  $\alpha$  at different chemical potentials. We set the model parameters as  $\lambda_{\parallel} = 0.41$  eV,  $\lambda_{\perp} = 0.44$  eV,  $t_{\parallel} = 0.566$  eV,  $t_{\perp} = 0.4$  eV,  $m_0 = 0.28$  eV,  $a = b = 1$  nm and  $c = 0.5$  nm if there is no specific indication [32]. The thickness  $L_z = 22$  and the magnetic layers  $m_z = 6$ . 1QL is about  $2c = 1nm$ .

The energy dispersions are  $E_{n,\chi,\pm} = \pm \sqrt{\lambda_{\parallel}^2(\sin^2 k_x + \sin^2 k_y) + \tilde{m}_{n,\chi}^2}$  in which  $\tilde{m}_{n,\chi}$  plays a role of momentum-dependent mass term for the Dirac fermions.

In the absence of magnetic doping, i.e.,  $\alpha = 0$ ,  $H_{1D}$  can be solved exactly. For details, the solutions of the energy and wave function can be seen in Ref. [37]. The masses have a relation  $\tilde{m}_{n,+} = -\tilde{m}_{n,-} = m_n$ , which gives rise to double degeneracy in the band structure rooted in combination of the time-reversal symmetry and inversion symmetry. For  $m(\mathbf{k}) > 0$ ,  $H_{1D}$  is topologically nontrivial, and has zero energy modes  $m_1 = 0$ ; for  $m(\mathbf{k}) < 0$ ,  $H_{1D}$  is topologically trivial, and the lowest energy modes  $m_1 = m(\mathbf{k})$ . Here the film is thick enough such that the finite size effect can be ignored [39]. Therefore, in Eq. (2),  $n = 1$  corresponds to the pair of gapless bands shown in Fig. 2. The spatial distribution of the wave function of  $m_1 = 0$  is mainly concentrated near the top and bottom surfaces as expected. The states of nonzero  $m_1$  or at large  $k$  are spatially distributed in the bulk, which represents that the surface states evolve into the bulk states with the variation of the wave vector  $\mathbf{k}$ . Here the complete band structure of the gapless Dirac fermions in the entire Brillouin zone consists of the surface electrons for  $m(\mathbf{k}) > 0$  or small  $\mathbf{k}$  and those extended in the  $z$  direction for  $m(\mathbf{k}) < 0$  or large  $\mathbf{k}$  (see in Fig. 3a). For  $n \geq 2$ , all  $m_n(\mathbf{k})$  at  $\mathbf{k} = 0$  are not equal to zero, which means the energy bands  $E_{n,\chi}$  open an energy gap at the point (see Section SI in Ref. [37]). For a small  $\mathbf{k}$ ,  $h_{n,\chi}(\mathbf{k}) \simeq \lambda_{\parallel}(k_x\sigma_x +$

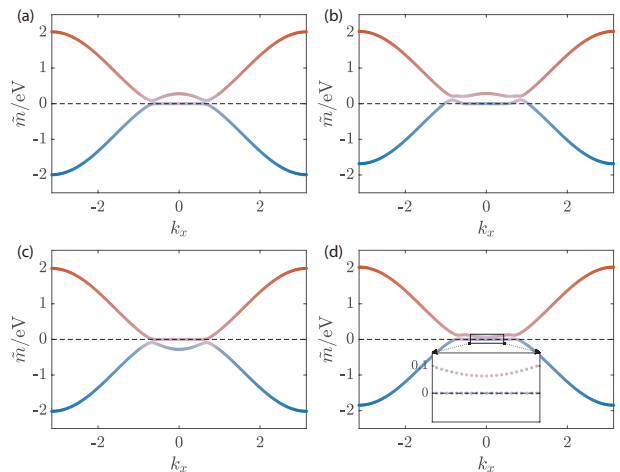


Figure 3. The evolution of the effective mass  $\tilde{m}_{n,\chi}(k_x, k_y = 0)$  ( $n = 1, 2$ ).  $\tilde{m}_{1,\chi}$  and  $\tilde{m}_{2,\chi}$  (a) with  $\chi = +$  at  $\alpha = 0$ , (b) with  $\chi = +$  at  $\alpha = 0.9$ ; (c) with  $\chi = -$  at  $\alpha = 0$ , (d) with  $\chi = -$  at  $\alpha = 0.9$ .

$k_y\sigma_y) + \chi m_n(0)\sigma_z$ . In other words, all the bands can be regarded as massive Dirac fermions.

In the presence of magnetic doping, the Zeeman field  $V_Z$  will change the band structures by altering effective mass  $\tilde{m}$ , while linear part vertical to  $z$ -direction remains unchanged due to degrees of freedom decoupling. In the basis of the energy eigenstates of  $H_{1D}(\alpha)$  at  $\alpha = 0$ , the Zeeman term can be expressed as  $\alpha \mathbf{I}_S(\mathbf{k})\tau_0\sigma_z$ , where  $\mathbf{I}_S(\mathbf{k})$  is a  $L_z \times L_z$  matrix (see Section SII in Ref. [37]) computable numerically. Thus  $H_{1D}$  is projected into the form  $\left(\bigoplus_{n=1}^{L_z} m_n\tau_z + \alpha \mathbf{I}_S(\mathbf{k})\tau_0\right)\sigma_z$ , and further diagonalizing this provides a bijection which maps the projected Hamiltonian form into the mass term  $\bigoplus_n \tilde{m}_{n,\chi}(\mathbf{k}, \alpha)\sigma_z$ . Confining to the subspace with  $\sigma_z = +$ , we could then track the evolution and interaction of the mass terms  $\tilde{m}_{n,\chi}$  between  $n = 1$  and  $n = 2$  blocks with increasing  $\alpha$  for given  $\chi$ . What stands out in the process is an exotic grafting behavior signed in Fig. 3: viewing from left to right, while the masses  $\tilde{m}_{n,+}$  ( $n = 1, 2$ ) maintain their shapes,  $\tilde{m}_{n,-}$  ( $n = 1, 2$ ), which represent one massless Dirac cone plus one massive Dirac cone, will fully exchange their low-energy parts with increasing  $\alpha$ , i.e., *massless*  $\longleftrightarrow$  *massive*. By increasing  $\alpha$ ,  $\tilde{m}_{n=1,-}$  and  $\tilde{m}_{n=2,-}$  behave as if they cross around  $\alpha_c \approx 0.74$  and then separate, during which detailed dynamic exchange reveals (see Section SV in Ref. [37]). On the other hand, what essentially remains unchanged is the high-energy part of each cone. Then since  $\tilde{m}_{n,\chi}$  of  $n = 1, 2$  are naturally assigned with opposite signs for their high-energy parts, viewing from a low-energy perspective, their high-energy masses exchange between massless and massive cones. The induced mass exchange of the massless and massive Dirac fermions is closely associated with the sign change of the Hall conductance.

*Quantized Hall conductance-* The Hamiltonian in Eq. 2 can be expressed in terms of the spin texture  $\mathbf{d} = (\lambda_{\parallel} \sin k_x, \lambda_{\parallel} \sin k_y, \tilde{m}_{n,\chi}(k_x, k_y))/E_{n,+}$ ,  $h_{n,\chi} = E_{n,+} \mathbf{d}(\mathbf{k}) \cdot \boldsymbol{\sigma}$ . Using the Kubo formula, the Hall conductance is given by

$$\sigma_H = -\frac{e^2}{h} \frac{1}{4\pi} \int \frac{dk_x dk_y}{4\pi} \mathbf{d} \cdot [\partial_{k_x} \mathbf{d} \times \partial_{k_y} \mathbf{d}] (f_{k,+} - f_{k,-}) \quad (3)$$

where  $f_{k,\pm} = \Theta(\mu - E_{n,\pm})$  is the Heaviside step function for Fermi-Dirac distribution at zero temperature and  $\mu$  is the chemical potential [7, 40]. For the massive Dirac fermions, the values of  $\tilde{m}_{n,\chi}$  at  $\mathbf{k} = (0, 0)$  and  $\mathbf{k} = (\pi, \pi)$  have the same sign, and there does not exist band inversion in the first Brillouin zone. The bands are always topologically trivial such that the fully filled bands, i.e.,  $\mu = 0$ , always have no Hall conductance which is consistent with the TKNN theorem [10]. For massless Dirac fermions,  $\tilde{m}_{n,\chi} = 0$  near  $\mathbf{k} = 0$ . In the regime,  $\mathbf{d} \cdot [\partial_{k_x} \mathbf{d} \times \partial_{k_y} \mathbf{d}] = 0$  which indicates that the Berry curvature of the band vanishes. Nonzero Berry curvature comes only from the part of nonzero  $\tilde{m}_{n,\chi}$  or the regime of large  $k$ . The Hall conductance is half-quantized for  $\mu$  located within the regime of  $\tilde{m}_{n,\chi} = 0$ ,  $\sigma_H = \frac{e^2}{2h} \text{sgn}[\tilde{m}_{n,\chi}(\pi, \pi)]$ . The quantization is protected by the emergent parity symmetry near the Fermi surface [29, 30].

Based on the mass-exchange picture, we have a theoretical explanation of the change of the Hall conductance induced by the Zeeman field in Fig. 2(c), (d). The film hosts a series of massive and massless Dirac fermions. For our purpose, we focus on the bands of  $n = 1$  and  $n = 2$  as all other massive Dirac fermions ( $n \geq 3$ ) have no contribution to the Hall conductance when they are fully filled for the chemical potential near  $\mu = 0$ . In the absence of the Zeeman field, the film hosts a pair of massless Dirac fermions, between which one has  $+\frac{e^2}{2h}$  and the other has  $-\frac{e^2}{2h}$  due to the sign difference of the mass terms at large  $k$ . The total Hall conductance is zero as expected. The presence of a weak Zeeman field does not change this situation. Nevertheless, equipped with a holistic view, when increasing the Zeeman field further, one massless Dirac fermion and one massive Dirac fermion exchange their low-energy masses, meanwhile their higher energy parts remain unchanged, but have different signs. Equivalently, the massless Dirac fermion changes the sign of massive term at higher energy viewed from a low-energy perspective. Consequently, its Hall conductance changes from  $+\frac{e^2}{2h}$  from  $-\frac{e^2}{2h}$ . During the process, the other massless Dirac Fermion remains its minus half-quantized Hall conductance unchanged, and the addition of two massless Dirac fermions gives a quantized Hall conductance  $-\frac{e^2}{2h} - \frac{e^2}{2h} = -\frac{e^2}{h}$ .

*Absence of chiral edge states* There are no chiral edge states around the system boundary in these paired gapless Dirac fermions. The quantum Hall conductance is

not governed by the Chern number and does not satisfy the conventional bulk-edge correspondence [12]. We calculated the local density states at the  $y$ -front surface of a  $y$ -opened film in Fig. 4(a), where there is clearly no dispersion that connects the lateral surface valence and conduction bands, opposite to the conventional case. This illustrates explicitly that there do not exist chiral edge states along the system boundary. The asymmetric local density of states between  $k_x$  and  $-k_x$  reflects the fact that there exists chiral edge current for the filled bulk states. The states carrying chiral edge current gradually becomes prominent when immersing into middle of  $z$  from its top surface. Furthermore, it is found that there still exists a chiral edge current whose amplitude is proportional to the chemical potential due to the time-reversal symmetry breaking caused by the Zeeman coupling [28]. As the Zeeman field is parallel with the lateral surface, the lateral surface states remain gapless. We present the spatial distribution of the electric current density in Fig. 4(b). It shows that the current density is mainly distributed around the surface of the magnetic layers, and decays quickly into the bulk, which demonstrates that the electronic transport mainly occurs on the surface. The local current density on the surface in Fig. 4(c) shows that the current density on the surface decays slowly which obviously deviates the exponential law. We fit the numerical result by using the current formula  $j_x(x) \propto J_1(2k_F x)/x$  in Ref. [28].  $J_1(x)$  is the first Bessel function. Small deviation appears within expectation as  $\alpha$  is finite, the overall shape which hints a power-law decay away from ends along  $y$  direction, however, is also clear, as indicated in Fig. 4(c). Also, it is worth of stressing that the current is induced by the Zeeman exchange interaction, and should be dissipationless. Such behavior depends heavily on the metallic nature of surface Dirac cone.

*Discussion-* In the field theory, the massless Dirac fermions possess the parity symmetry. When the Dirac fermions are coupled to electromagnetic field, its action fails to restore the symmetry in any regularization, and is characterized by a half-quantized Hall conductance. The discussion on parity anomaly in the condensed matter dated back to early 1980s [41–43]. It has attracted extensive interests since the discovery of TIs as the massless Dirac fermions can exist on the surface [44–46]. The film here provides a platform to explore the related physics of parity anomaly. The massless Dirac fermions on the surfaces accompany with presence of nonzero zero term  $\tilde{m}_{n,\chi}$  at large  $k$ , which plays a role of the regulators of Dirac fermions in the field theory. Thus the nonzero Hall conductance is just determined by the sign of  $\tilde{m}_{n,\chi}$  at  $k = 0$  and large  $k$ , and independent of the specific form and the amplitude of  $\tilde{m}_{n,\chi}$ . In this sense, the present work reflects the physics of quantum anomaly. However, we should keep in mind that the term has already broken the parity symmetry explicitly.

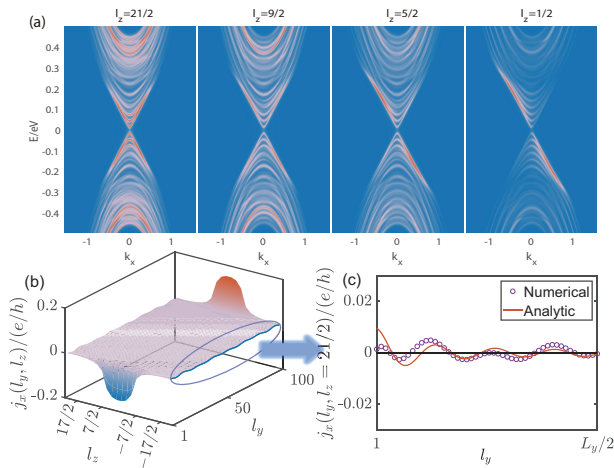


Figure 4. The local density of states and local current distribution of the film with  $L_z = 22$ , and  $\alpha = 0.8$ . The lattice site  $l_z = \pm 1/2; \dots; \pm(L_z - 1)/2$  and  $l_y = 1, \dots, L_y$  (a) Local density of state  $\rho(l_z, k_x, E)$  at the  $y$ -front of the film with width  $L_y = 20$ . Several representative  $l_z$  are picked out to show the absence of chiral edge states. (b) The local current density  $j_x(l_y, l_z)$  for a film with width  $L_y = 100$ . The chemical potential  $\mu = 0.1eV$ . (c) The surface current density as a function of  $l_y$  at the surface  $l_z = 21/2$  or  $-21/2$ ,  $j_x(l_y, l_z = 21/2)$ , compared with the current formula  $j_x(x) \propto J_1(2k_{Fx})/x$  [28].

This work was supported by the Research Grants Council, University Grants Committee, Hong Kong under Grant Nos. C7012-21G and 17301823 and the National Key R&D Program of China under Grant No. 2019YFA0308603.

\* sshen@hku.hk

[1] F. D. M. Haldane, Phys. Rev. Lett. **61**, 2015 (1988).  
 [2] R. Yu, W. Zhang, H.-J. Zhang, S.-C. Zhang, X. Dai, and Z. Fang, Science **329**, 61 (2010).  
 [3] Z. Qiao, S. A. Yang, W. Feng, W.-K. Tse, J. Ding, Y. Yao, J. Wang, and Q. Niu, Phys. Rev. B **82**, 161414(R) (2010).  
 [4] R.-L. Chu, J. Shi, and S.-Q. Shen, Phys. Rev. B **84**, 085312 (2011).  
 [5] C.-X. Liu, S.-C. Zhang, and X.-L. Qi, Annu. Rev. Condens. Matter Phys. **7**, 301 (2016).  
 [6] C.-Z. Chang, C.-X. Liu, and A. H. MacDonald, Rev. Mod. Phys. **95**, 011002 (2023).  
 [7] S.-Q. Shen, *Topological Insulators*, 2nd ed., Vol. 187 (Springer, Singapore, 2017).  
 [8] B. I. Halperin, Phys. Rev. B **25**, 2185 (1982).  
 [9] B. I. Halperin, Rev. Mod. Phys. **92**, 045001 (2020).  
 [10] D. J. Thouless, M. Kohmoto, M. P. Nightingale, and M. den Nijs, Phys. Rev. Lett. **49**, 405 (1982).  
 [11] Q. Niu, D. J. Thouless, and Y.-S. Wu, Phys. Rev. B **31**, 3372 (1985).  
 [12] Y. Hatsugai, Phys. Rev. Lett. **71**, 3697 (1993).  
 [13] C.-Z. Chang, J. Zhang, X. Feng, J. Shen, Z. Zhang, M. Guo, K. Li, Y. Ou, P. Wei, L.-L. Wang, et al., Science

**340**, 167 (2013).  
 [14] C.-Z. Chang, W. Zhao, D. Y. Kim, H. Zhang, B. A. Assaf, D. Heiman, S.-C. Zhang, C. Liu, M. H. Chan, and J. S. Moodera, Nat. Mater. **14**, 473 (2015).  
 [15] J. Checkelsky, R. Yoshimi, A. Tsukazaki, K. Takahashi, Y. Kozuka, J. Falson, M. Kawasaki, and Y. Tokura, Nat. Phys. **10**, 731 (2014).  
 [16] X. Kou, S.-T. Guo, Y. Fan, L. Pan, M. Lang, Y. Jiang, Q. Shao, T. Nie, K. Murata, J. Tang, et al., Phys. Rev. Lett. **113**, 137201 (2014).  
 [17] Y. Okazaki, T. Oe, M. Kawamura, R. Yoshimi, S. Nakamura, S. Takada, M. Mogi, K. S. Takahashi, A. Tsukazaki, M. Kawasaki, Y. Tokura, and N.-H. Kaneko, Nat. Phys. **18**, 25 (2022).  
 [18] J. Li, Y. Li, S. Du, Z. Wang, B.-L. Gu, S.-C. Zhang, K. He, W. Duan, and Y. Xu, Sci. Adv. **5**, eaaw5685 (2019).  
 [19] Y. Deng, Y. Yu, M. Z. Shi, Z. Guo, Z. Xu, J. Wang, X. H. Chen, and Y. Zhang, Science **367**, 895 (2020).  
 [20] M. M. Otrokov, I. I. Klimovskikh, H. Bentmann, D. Estyunin, A. Zeugner, Z. S. Aliev, S. Gaß, A. Wolter, A. Koroleva, A. M. Shikin, et al., Nature **576**, 416 (2019).  
 [21] C. Liu, Y. Wang, H. Li, Y. Wu, Y. Li, J. Li, K. He, Y. Xu, J. Zhang, and Y. Wang, Nat. Mater. **19**, 522 (2020).  
 [22] Y. Gong, J. Guo, J. Li, K. Zhu, M. Liao, X. Liu, Q. Zhang, L. Gu, L. Tang, X. Feng, et al., Chin. Phys. Lett. **36**, 076801 (2019).  
 [23] Y. J. Chen, L. X. Xu, J. H. Li, Y. W. Li, H. Y. Wang, C. F. Zhang, H. Li, Y. Wu, A. J. Liang, C. Chen, S. W. Jung, C. Cacho, Y. H. Mao, S. Liu, M. X. Wang, Y. F. Guo, Y. Xu, Z. K. Liu, L. X. Yang, and Y. L. Chen, Phys. Rev. X **9**, 041040 (2019).  
 [24] B. Chen, F. Fei, D. Zhang, B. Zhang, W. Liu, S. Zhang, P. Wang, B. Wei, Y. Zhang, Z. Zuo, et al., Nat. Communi. **10**, 4469 (2019).  
 [25] M. Liu, W. Wang, A. R. Richardella, A. Kandala, J. Li, A. Yazdani, N. Samarth, and N. P. Ong, Sci. Adv. **2**, e1600167 (2016).  
 [26] K. Yasuda, M. Mogi, R. Yoshimi, A. Tsukazaki, K. Takahashi, M. Kawasaki, F. Kagawa, and Y. Tokura, Science **358**, 1311 (2017).  
 [27] M. Mogi, Y. Okamura, M. Kawamura, R. Yoshimi, K. Yasuda, A. Tsukazaki, K. Takahashi, T. Morimoto, N. Nagaosa, M. Kawasaki, et al., Nat. Phys. **18**, 390 (2022).  
 [28] J.-Y. Zou, B. Fu, H.-W. Wang, Z.-A. Hu, and S.-Q. Shen, Phys. Rev. B **105**, L201106 (2022).  
 [29] J.-Y. Zou, R. Chen, B. Fu, H.-W. Wang, Z.-A. Hu, and S.-Q. Shen, Phys. Rev. B **107**, 125153 (2023).  
 [30] B. Fu, J.-Y. Zou, Z.-A. Hu, H.-W. Wang, and S.-Q. Shen, npj Quantum Mater. **7**, 94 (2022).  
 [31] Y. Tokura, K. Yasuda, and A. Tsukazaki, Nat. Rev. Phys. **1**, 126 (2019).  
 [32] H. Zhang, C.-X. Liu, X.-L. Qi, X. Dai, Z. Fang, and S.-C. Zhang, Nat. Phys. **5**, 438 (2009).  
 [33] Y. Chen, J.-H. Chu, Z. Liu, S.-K. Mo, H. Zhang, D. Lu, et al., Science **325**, 178 (2009).  
 [34] Y. Zhang, K. He, C.-Z. Chang, C.-L. Song, L.-L. Wang, X. Chen, J.-F. Jia, Z. Fang, X. Dai, W.-Y. Shan, et al., Nat. Phys. **6**, 584 (2010).  
 [35] Y.-F. Zhao, R. Zhang, R. Mei, L.-J. Zhou, H. Yi, Y.-Q. Zhang, J. Yu, R. Xiao, K. Wang, N. Samarth, et al., Nature **588**, 419 (2020).  
 [36] C.-X. Liu, X.-L. Qi, H. J. Zhang, X. Dai, Z. Fang, and S.-C. Zhang, Phys. Rev. B **82**, 045122 (2010).

- [37] See Supplemental Material at [URL to be added by publisher] for details of SI: Derivation of Eq.(2) at  $\alpha = 0$ , SII: The Zeeman term, SIII: Case study of conventional anomalous Hall effect, SIV: Case study of  $\alpha = 0.9$  explained by only  $n - 1, 2$ , and SV: Fine process near transition, which includes Refs. [XXX].
- [38] G. Mahan, *Many-particle physics* (Plenum Press, New York, NY, 1981).
- [39] H.-Z. Lu, W.-Y. Shan, W. Yao, Q. Niu, and S.-Q. Shen, Phys. Rev. B **81**, 115407 (2010).
- [40] X.-L. Qi, T. L. Hughes, and S.-C. Zhang, Phys. Rev. B **78**, 195424 (2008).
- [41] A. J. Niemi and G. W. Semenoff, Phys. Rev. Lett. **51**, 2077 (1983).
- [42] A. N. Redlich, Phys. Rev. Lett. **52**, 18 (1984).
- [43] E. Fradkin, E. Dagotto, and D. Boyanovsky, Phys. Rev. Lett. **57**, 2967 (1986).
- [44] S. Zhang, L. Pi, R. Wang, G. Yu, X.-C. Pan, Z. Wei, J. Zhang, C. Xi, Z. Bai, F. Fei, et al., Nat. Communi. **8**, 977 (2017).
- [45] J. Bottcher, C. Tutschku, L. W. Molenkamp, and E. M. Hankiewicz, Phys. Rev. Lett. **123**, 226602 (2019).
- [46] H.-W. Wang, B. Fu, and S.-Q. Shen, Phys. Rev. B **104**, L241111 (2021).